Semiconductor Nanowire Optical Antenna Solar Absorbers

Linyou Cao,[†] Pengyu Fan,[†] Alok P. Vasudev,[†] Justin S. White,[†] Zongfu Yu,[‡] Wenshan Cai,[†] Jon A. Schuller,[†] Shanhui Fan,[‡] and Mark L. Brongersma*,[†]

[†]Geballe Laboratory for Advanced Materials, Stanford University, California 94305 and [‡]Ginzton Laboratory, Stanford University, California 94305

ABSTRACT Photovoltaic (PV) cells can serve as a virtually unlimited clean source of energy by converting sunlight into electrical power. Their importance is reflected in the tireless efforts that have been devoted to improving the electrical and structural properties of PV materials. More recently, photon management (PM) has emerged as a powerful additional means to boost energy conversion efficiencies. Here, we demonstrate an entirely new PM strategy that capitalizes on strong broad band optical antenna effects in one-dimensional semiconductor nanostructures to dramatically enhance absorption of sunlight. We show that the absorption of sunlight in Si nanowires (Si NWs) can be significantly enhanced over the bulk. The NW's optical properties also naturally give rise to an improved angular response. We propose that by patterning the silicon layer in a thin film PV cell into an array of NWs, one can boost the absorption for solar radiation by 25 % while utilizing less than half of the semiconductor material (250 % increase in the light absorption per unit volume of material). These results significantly advance our understanding of the way sunlight is absorbed by one-dimensional semiconductor nanostructures and provide a clear, intuitive guidance for the design of efficient NW solar cells. The presented approach is universal to any semiconductor and a wide range of nanostructures; as such, it provides a new PV platform technology.

KEYWORDS Solar cell, semiconductor nanowires, optical antennas, photon management, light trapping

The large-scale implementation of PV technology around the world would greatly benefit from further cost reductions in the manufacturing of solar modules.[1] Moreover, it is essential to identify new ways to reduce the amount of semiconductor material used in PV cells, particularly for those cells employing non-earth-abundant elements like indium (CuInGaSe or CIGS cells) or tellurium (CdTe cells). Whereas thin film PV offers a viable pathway to reduce fabrication costs and material usage,[2] their energy conversion efficiencies can still be improved significantly by enabling them to harness a larger fraction of the incident solar photons. As a result, researchers are frantically searching for new approaches to dramatically boost the amount of light absorption per unit volume of semiconductor. In addition to conventional antireflection coatings, reflective substrates, and textured surfaces,[2–6] more advanced light trapping techniques based on resonant cavities,[7] plasmonics,[8] and photonic crystals[5,9] have recently gained significant interest. The best imaginable PM technology would effectively trap and/or concentrate light in a broad-band, angle-independent, and polarization-independent fashion. Resonant PM structures have demonstrated significant promise, but their performance is typically limited by a fundamental trade-off between the attainable absorption enhancement and their operational bandwidth. Moreover, resonant structures tend to exhibit a strongly angle-dependent optical response and the resulting solar cells require bulky solar tracking systems to follow the sun's movement in order to maximize their daily energy output. The fabrication of more advanced PM structures that could mitigate some of these issues is typically expensive, and the increased cost offsets the potential performance gains. Here, we demonstrate that the use of optical antenna effects in one-dimensional semiconductor nanostructures enables significant enhancement in the absorption of sunlight with little dependence on illumination angle. As sufficiently large diameter (about 100 nm or more) NWs are known to also exhibit a polarization-independent response,[10] they could serve as an almost ideal building block for PV systems. Building on this notion, we propose a new type of high-performance PM strategy for solar cells in which a thin semiconductor film is patterned into an array of thoughtfully engineered one-dimensional nanostructures. The most important benefits of this new PM strategy are the ease of fabrication and the broad band nature of the absorption enhancement which is derived from the plurality of optical resonances in the wires that cover the solar spectrum.

Arrays of semiconductor nanostructures with elongated shapes, such as NWs, nanorods, and nanopillars, have recently demonstrated significant promise for photovoltaic applications; these structures can exhibit both enhanced absorption and a reduced reflectivity as compared to planar, film-based devices.[11–14] Our understanding of the NW's optical response to solar radiation is still rapidly growing, and a deep fundamental knowledge of their optical properties is key to the design of future generations of high-performance NW solar cells. In this paper, we demonstrate
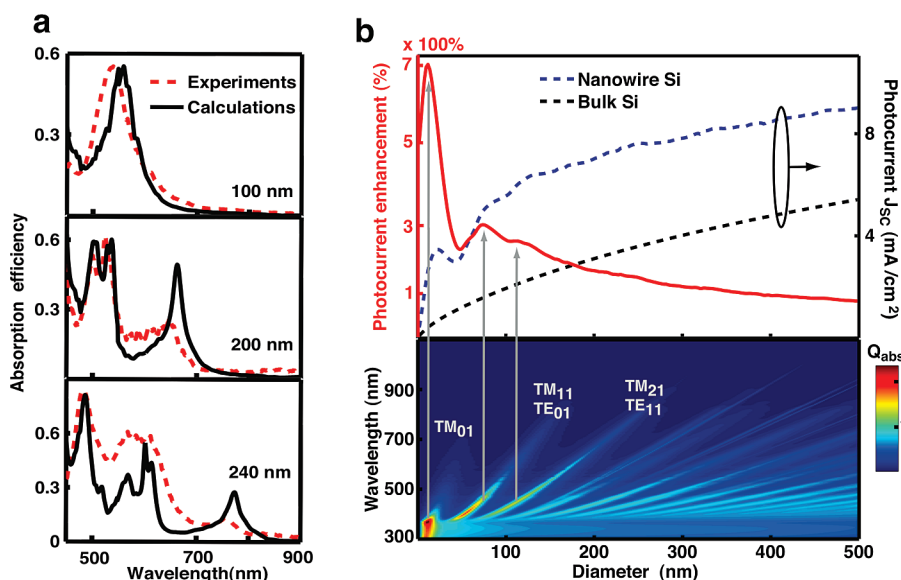
FIGURE 1. Leaky mode resonances (LMRs) and enhanced photocurrent density in silicon nanowires. (a) Measured (red dashed) and calculated (black solid) spectral absorption efficiency Q_{abs} of single Si nanowires with diameter of 100, 200, and 240 nm. The measured results were scaled by a constant factor over the entire spectrum to best fit the calculations. (b) (Upper) Calculated short-circuit photocurrent density J_{sc} for silicon nanowires (blue dash) and for bulk silicon (dark dash) of comparable thickness (for detail about the normalization see Figure S1 in the Supporting Information). The red solid line indicates the photocurrent enhancement of the nanowire per unit volume of material; the expression used to calculate the enhancement is $(J_{SC,NW}/V_{NW} - J_{SC,Bulk}/V_{Bulk})/(J_{SC,Bulk}/V_{Bulk})$. (Lower) Two-dimensional plot of the calculated absorption efficiency Q_{abs} of a crystalline silicon nanowire as functions of the wavelength and diameter. The distinct streaks of high intensity indicate the presence of the various leaky mode resonances, with the first three indexed. The gray arrows mark the one-to-one correlation between the leaky mode resonances and the photocurrent enhancement peaks.

that semiconductor NWs can effectively serve as a set of broad band optical antennas for sunlight. As such, the NWs capture and absorb significantly more solar photons than an equivalent volume of bulk material. Recently, powerful antenna effects were experimentally demonstrated in photocurrent measurements on Ge NWs[10] at specific wavelengths. When the illumination wavelength matched one of the allowed leaky mode resonances (LMRs), the high refractive index wire was able to capture and trap the light by multiple internal reflections from its boundary. As a consequence, light absorption and the resulting photocurrent could be enhanced at a desired wavelength by tuning the NW diameter. Here, we illustrate how light absorption in NWs can be increased over the tremendously broad band solar spectrum by taking advantage of the plurality of spectrally separated LMR resonances supported by relatively large (>100 nm) diameter structures. The nature of the antenna effects in NWs also naturally provides for a desirable weak angle- and polarization-dependence of the optical response.

In the following, we start with an experimental demonstration of optical antenna effects in individual Si NWs, which form the basic building blocks of our proposed PV cells. We then continue with an optimization of their absorption efficiencies by engineering the best possible match between the absorption spectrum of the wires and the solar spectrum. In this exercise we not only show large absorption enhancements compared to planar structures, but we also experimentally demonstrate the broad angular response. We

continue by showing how this approach can be applied to a great diversity of materials systems (including, e.g., amorphous Si, CdTe, GaAs, CuInGeSe) and wire geometries of different cross-sectional shape (e.g., circular, rectangular, hexagonal, or triangular). We conclude by illustrating how the individual NW optimizations can be used to guide the design of large-area devices consisting of a plurality of NWs.

In order to demonstrate the superior optical properties of one-dimensional semiconductor nanostructures over films, we fabricated a set of metal−semiconductor−metal (MSM) photodetectors with individual crystalline SiNWs (c-SiNWs). The c-SiNWs were grown by a gold-catalyzed chemical vapor deposition procedure,[15] and spectral absorption properties of the NWs were derived from photocurrent measurements. The measured photocurrent spectra for several c-SiNWs of different diameter are given in Figure 1a. The figure also shows the predicted absorption spectra for cylindrical NWs based on the well-established Lorentz−Mie light scattering formalism[16] (for details see Supporting Information, section I). In order to compare the experimental and theoretical results, both data sets are given in terms of the spectral absorption efficiency, Q_{abs}, which is defined as the absorption cross section normalized to the geometrical cross section of the NW. Distinct peaks can be observed in the Q_{abs} spectra that exhibit a substantial dependence on the NW size, consistent with the excitation of LMRs.[10] The good agreement between the experimental and calculated spectra suggests that the LMR-enhanced absorption in the NWs can be approximated by the Lorentz−Mie formalism and by

assuming a homogeneous host medium of unity refractive index. It should be mentioned that this formalism is exact for NWs embedded in a uniform medium, but it does not take into account the presence of a substrate. As such, this theory has a good predictive power when the optical fields of the resonant mode are highly confined to within the wire. In reality, the optical mode modes supported by nanowires extend noticeably outside of the wire and differences between experiment and theory can be expected. This effect is strongest for larger nanowires in which the lowest order optical modes extends most significantly outside of the nanowire. This explains for example the differences in the experimental and theoretical spectra near 680 nm for the 200 nm nanowire. A similar phenomenon was observed in germanium nanowires (see Supporting Information of ref 10). Although even better agreement can be obtained using more time-consuming full-field simulations that include the presence of a substrate,[10] the analytic Lorentz–Mie theory allows for a rapid first-order optimization of the NW-based PV cells discussed below.

In order to optimize PV performance with LMRs, we first aim to identify the optimum SiNW diameter, d, that will maximize the absorption of sunlight. To this end, we calculate $Q_{abs}(\lambda, d)$ for SiNWs of different diameters and integrate the calculated absorption efficiencies with the spectral photon flux density delivered by the sun,[17] $F_s(\lambda)$. This integral equals the number of absorbed solar photons per unit time and exposed surface area of a single NW. To evaluate the possible benefits of these NWs in future solar cell devices, it is of value to also provide the commonly used short-circuit photocurrent density of the NW, $J_{SC}(d) = q \int F_s(\lambda) Q_{abs}(\lambda, d) d\lambda$. Here, q is the charge carried by one electron. In this equation the internal quantum efficiency (IQE) was assumed to be 100%, which has recently been demonstrated with NW junction devices.[18] The current density refers to the photocurrent divided by the projected area of the NW (dl, where l is the length of the NW).[18] In order to make a comparison to planar Si structures, we have also calculated the absorption of light in a surface layer of a crystalline Si wafer with the same thickness as the wire. For these calculations, we have used the well-established optical properties of single-crystalline silicon.[19] As shown in the upper panel of Figure 1b, the NW produces a much larger photocurrent density than that of bulk Si for the same volume of material. For example, an 80 nm diameter NW experiences a 300% enhancement in the photocurrent per unit volume.

The role of the LMRs in the enhancement can clearly be seen in a two-dimensional plot of the absorption efficiency Q_{abs} versus λ and d (Figure 1b lower panel). This figure shows the absorption enhancements related to the various transverse electric (TE_{ml}) and transverse magnetic (TM_{ml}) LMRs of a NW illuminated under normal incidence, where m and l are the azimuthal mode number and radial order of the resonances, respectively.[10] A comparison between the upper and lower panels of Figure 1b reveals a one-to-one cor-

respondence between the peaks in the photocurrent enhancement and the spectral locations of the LMRs. As illustrated by the gray arrows in Figure 1b, the first enhancement peak (the enhancement peaks are counted as first, second, third, etc., in the order of ascending diameter) finds its origin in the excitation of the lowest order LMR, TM_{01}. This peak is seen in NWs that are very small (~10 nm) compared to the wavelengths from the incident sun light; it arises from an electrostatic dipole excitation of the wire (see Supporting Information section II). The second and the third photocurrent peaks can be correlated to the following higher order LMRs, TM_{11}/TE_{01} and TM_{21}/TE_{11}, respectively. From this analysis, the role of the various LMRs in enhancing the photocurrent and thus the PV performance is evident.

The LMRs not only enhance the NW's ability to absorb sunlight but also can substantially minimize the dependence of the light absorption on illumination angle. Due to the cylindrical symmetry, a change in the illumination angle in the plane normal to the wire does not affect the light absorption. Figure 2a shows the calculated photocurrent density J_{sc} for different SiNW diameters as a function of the angle between the illumination direction and the NW axis (normal incidence corresponds to 90°). To highlight the angle dependence of the photocurrent, the angular spectra were normalized to the maximum current obtained for each diameter. Figure 2b also shows linecuts from Figure 2a for four selected NW diameters (indicated by the dashed vertical lines) and for planar Si. We can see that the photocurrent in the NW generally shows less dependence on the incident angle than that of a planar structure except for very small (~20 nm) wires. For the coming discussion, it is worth noting that NWs with diameters of ~80–100 nm exhibit a particularly small dependence of J_{sc} on incident angle; their photocurrent is more-or-less constant until the incident angle is less than 20°.

The angle dependence of the NW photocurrent can be understood from the angle dependence in the excitation of LMRs. This angle dependence absorption has intuitive geometric contributions and more complex materials contributions, which result from dispersion. In order to selectively explore the effects of geometry, we plot the absorption efficiency Q_{abs} as a function of a dimensionless size parameter $nkd/2$ (k, wavevector of the incident light in free space) and the illumination angle for a frequency-independent refractive index, $n = 4 + 0.03i$. The index values are representative of a high-index, absorbing semiconductor NW. The result is shown in Figure 2c, and relevant LMRs that contribute to Q_{abs} are indicated as well. Among all the LMRs, we can find that the first-order LMRs show a significant change with the angle, while the second-order LMRs exhibit the weakest angle dependence and the angle dependence is quite small for higher LMRs as well. On the basis of the previous results, it is natural to expect a substantial absorption enhancement and a weak angle dependence in the response of SiNW solar cells when the second-order LMRs
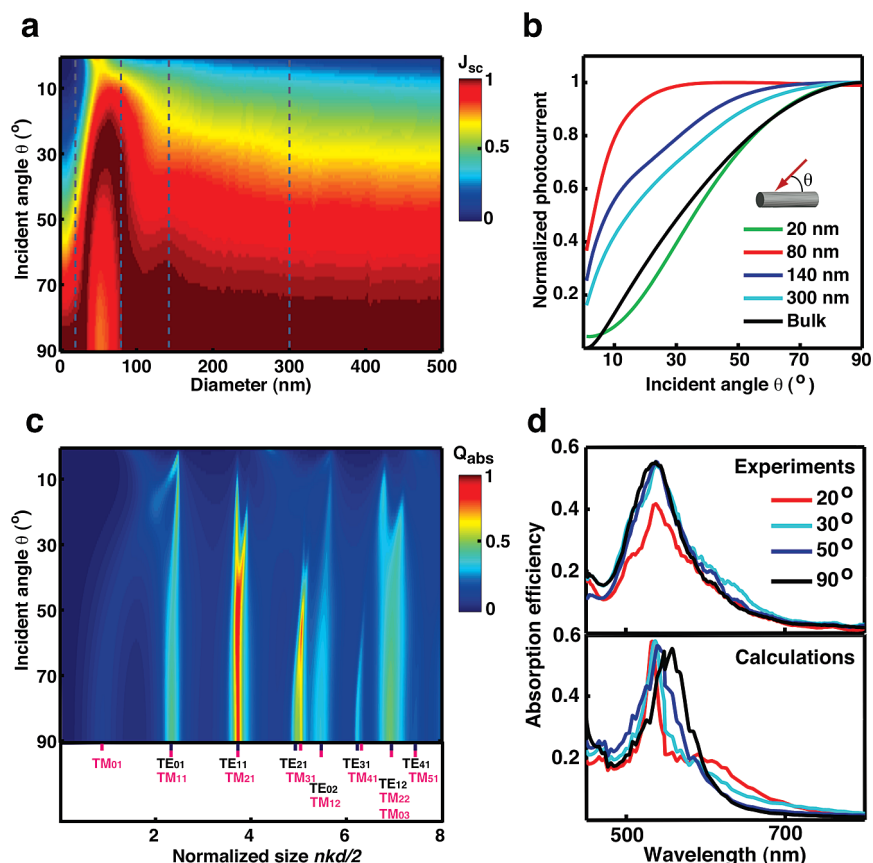
FIGURE 2. Dependence of the photocurrent density and LMRs in silicon nanowires on the illumination angle. (a) Two-dimensional plot of the normalized J_{sc} of silicon nanowires as a function of the diameter and the incident angle. The photocurrent for each nanowire is normalized to the value at normal incidence to emphasize the angle dependence. The gray dashed lines indicate four representative results replotted in (b). (b) Dependence of the normalized J_{sc} on the illumination angle for various diameter (20, 80, 140, and 300 nm) silicon nanowires. The angle dependence of the photocurrent in planar bulk silicon is also given for comparison. (c) Two-dimensional plot of normalized absorption efficiency Q_{abs} of silicon nanowires as a function of the dimensionless normalized size parameter $nkd/2$ and the incident angle. In the calculation, the refractive index n is artificially set constant at $4 + 0.03i$ in order to selectively study the angle dependence of LMRs. The LMRs excited under normal illumination are indexed underneath, and the term of TE or TM should be changed to EH or HE for oblique incidence. (d) Measured (Upper) and calculated (Lower) absorption spectra of 100 nm diameter silicon nanowires illuminated at different incidence angles (20°, 30°, 50°, and 90°).

provide a large contribution to the absorption of sunlight. Figure 1b shows that c-SiNW sizes in the range from 80 to 100 nm provide a good wavelength match between the second-order LMRs resonance and the peak of the solar spectrum (near 500 nm). The anticipated weak angle dependence of the absorption in such SiNWs is confirmed by experimental and calculated absorption spectra on a 100 nm diameter c-SiNW, as shown in Figure 2d.

LMRs are essentially morphology-dependent resonances,[20] arising from the finite NW size and the large refractive index contrast of the NW with respect to its surroundings. It should thus be expected that any high-index semiconductor used in solar applications could benefit from these types of resonances. Figure 3a shows the calculated J_{sc} for normal-incidence illumination and corresponding enhancement for cylindrical nanowires made from popular semiconductors in solar applications, including germanium (Ge), amorphous silicon (α-Si), CdTe, CuInGaSe, and gallium arsenide (GaAs). All materials systems show significant

enhancements and similar trends in the dependence on the nanowire size. For all of the semiconductors, J_{sc} tends to show good enhancements and little angle dependence when the NW size is optimized to again match the second peak in the plots of photocurrent vs size (Figure 3b). For example, a 130 nm diameter α-Si NW may generate J_{sc} of ∼24 mA/cm^2 out of ∼49 mA/cm^2 that is available from the AM 1.5 spectrum.[17] For NWs larger than 100 nm, J_{sc} is approximately independent of size; these larger wires experience only minor gains in absorption at long wavelengths where the solar irradiance is relatively small (see Figure S3 of the Supporting Information).

Optical antenna resonances are not limited to a perfect cylindrical geometry and are a general feature of high-index nanostructures. Figure 4a shows the calculated J_{SC} for one-dimensional α-Si structures with hexagonal, rectangular, and triangular cross sections as a function of their size. Figure 4b plots the absorption efficiency spectra of these objects for a diameter matching the second size resonance in the
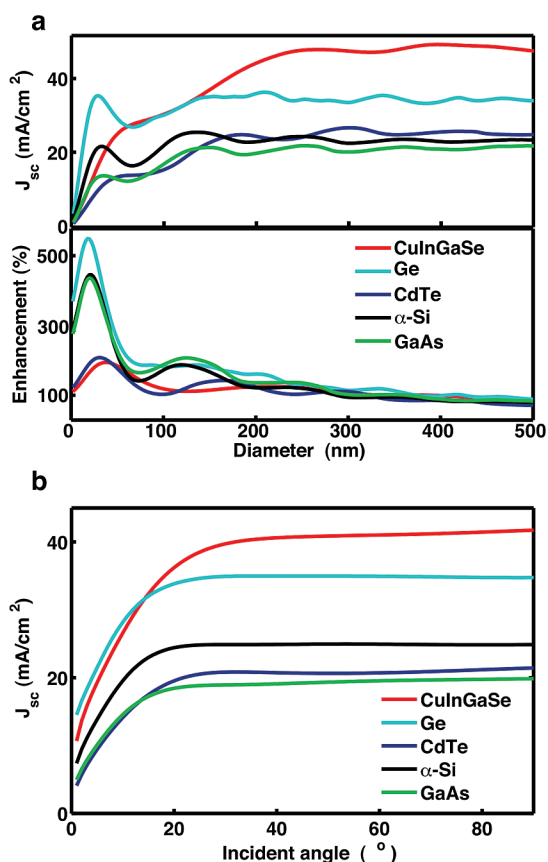
FIGURE 3. Generality of the photocurrent enhancement and minimized angle dependence of the photocurrent from individual semiconductor nanowires: (a) (upper) short circuit photocurrent density J_{sc} in nanowires of other major photovoltaic materials, including CuInGaSe, Ge, CdTe, amorpous Si, and GaAs, and (lower) photocurrent enhancement in the nanowires compared to their bulk counterparts. (b) Minimized dependence of J_{sc} of various semiconductor nanowires on the incident angle. The diameters of the nanowires are CuInGaSe, 180 nm, Ge, 140 nm, α-Si, 120 nm, CdTe, 140 nm, and GaAs, 120 nm, respectively. Those diameters match the excitation of the second-order LMRs.
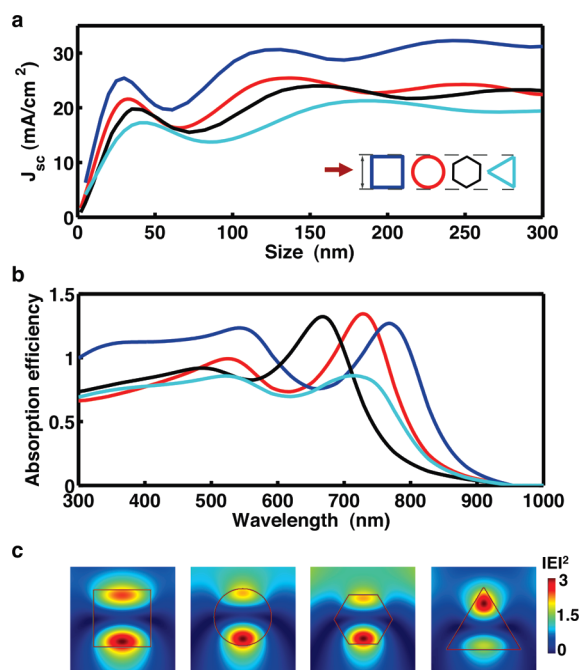

FIGURE 4. Generality of the optical resonance and short-circuit current enhancement to one-dimensional nanostructures. The simulations were performed using full-field electromagnetic simulations based on the finite difference frequency domain (FDFD) technique. (a) Simulated short-circuit photocurrent density J_{sc} for one-dimensional amorphous Si structures of circular, rectangular, hexagonal, and triangular cross section as a function of size. The inset schematic illustrates the way to compare the size for different structures, and the red arrow indicates the illumination geometry used in the calculations. (b) Simulated absorption spectra of these one-dimensional amorphous Si structures in a size lying in the regime that corresponds to their second enhancement peaks shown in (a). Specifically, the size is 180 nm for the triangular nanowire and 130 nm for all other structures. (c) Calculated electric field distribution (normalized to the incidence) of these structures upon the resonance corresponding to the absorption peak at ∼700 nm in (b).

photocurrent (between 100 and 200 nm depending on the cross-sectional shape). The results for a cylinder are also given for reference. The spectra are qualitatively very similar. They all feature large absorption efficiencies (close to unity) over a wide frequency range. The observed differences in Q_{abs} are primarily due to the different volumes of material in the structures. These results indicate that similar types of optical antenna resonances are excited in all the structures. The similarity of the optical resonances is further illustrated in Figure 4c, which shows the internal electric fields (only for TM illumination) for these structures at the absorption resonance near 700 nm shown in Figure 4b. All field plots show two field maxima, similar to the TM_{11} LMR in cylinders.[10] This similarity indicates that the low-order leaky mode resonances are quite insensitive to the specific morphology. This result is not necessarily intuitive as physical quantities often strongly depend on the nanostructure shape and size.

Our newly gained understanding of PM in individual NWs can now guide the rational design of high-efficiency NW-based PV cells. This is illustrated with a design employing an array of α-Si NWs on a glass substrate, as shown in the inset of Figure 5a. From the discussion of parts a and b of Figure 3, we learned that a 130 nm αSi NW shows both a high short circuit current and a broad angular response. We take this NW as a building block for a large NW array that could find application in a PV cell. If its antenna properties can be preserved in the array configuration, the NW array is expected to generate a substantially higher short circuit current than an unstructured film of the same thickness, despite the lower volume of semiconductor. In order to keep the discussion as general as possible, we calculate the NW array performance without making assumptions about the electrical design for the charge collection (e.g., p−n junction) nor do we make detailed assumptions about the electrical materials quality; we again simply assume a 100% internal quantum efficiency for the NWs. In order to compare the anticipated performance of a NW array to a conventional,
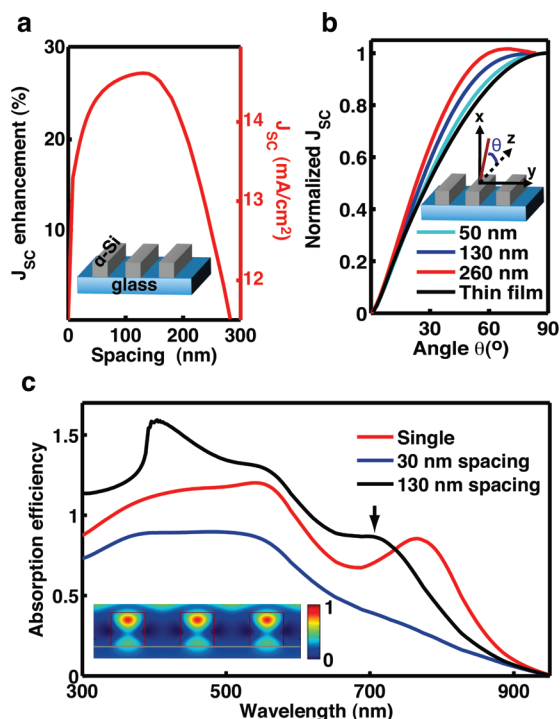
FIGURE 5. Photocurrent enhancement and optical resonances in rectangular nanowire arrays on glass. (a) Calculated photocurrent density J_{sc} of an array of 130 nm wide square nanowires as a function of the nanowire separation. The left-side vertical axis indicates the photocurrent normalized to that of a continuous film (zero separation). Inset, schematic illustration of the array structure. (b) Calculated dependence of the photocurrent density J_{sc} on the illumination angle for the array with various spacings (50, 130 and 260 nm) and a 130 nm thick film. The incident angle is changed in the xz plane, while the nanowires are aligned along the z axis. (c) Calculated absorption spectra of a 130 nm wide square nanowire in the array with different separations of 30 and 130 nm. The red line is the absorption spectra of a single nanowire on the same substrate. The broad absorption spectrum of the array with the 130 nm spacing strongly resembles that of a single nanowire. Inset, normalized intensity of electric field ($|E|^2$) distribution in the array corresponding to the peak marked by the vertical arrow (only TM polarization is given) with a linear color bar scaled from 0 to 1. It is worth noting that the absorption efficiency Q_{abs} of the nanowire array in (c) is normalized to the geometrical projected area of the nanowire (without taking into account the interspacing). This choice was made to enable a convenient comparison with the absorption enhancements in single nanowires. In contrast, J_{sc} in (a) is normalized to the total area of the cell, including both the area taken up by the nanowires and the space between the nanowires. This choice was made to enable fair comparisons between devices.

continuous thin film cell, we again calculate J_{sc}, this time by normalizing the photocurrent to the total area of the cell (including both the area taken up by the nanowires as well as the space between the nanowires). To visualize the transition from a continuous film to an array of well-separated NWs, we calculated the J_{sc} for a top-illuminated array of 130 nm rectangular NWs as a function of their spacing and compared it to the J_{sc} of a 130 nm thick film, 11.3 mA/cm² (Figure 5a). The optimum NW array with a spacing of 130 nm features a ~25% increase in J_{sc}, while using only 50% of the material (i.e., a 250% increase in current per unit volume material). The optimized J_{sc} is 14.5

mA/cm², accounting for a ~30% conversion efficiency of all solar radiation energy available in the AM 1.5 spectrum[17] (~49 mA/cm²). The physics behind the observed absorption enhancements at small NW spacings (~10 nm) is quite well-understood. Here, the incident wave couples to the waveguide modes of the original slab, which are weakly perturbed by the narrow slits between the NWs.[21,22] It has also been argued that at larger spacings the response of the individual NWs starts playing an increasingly important role.[21,23] This observation is important as it justifies our approach to first optimize the individual NW response and then to use the best NWs as building blocks for the array cell. Our data indeed indicate that the optical resonances seen in the individual NWs play an important role in enhancing the absorption of sunlight by the array. Their importance is first of all reflected in the weaker dependence of J_{sc} on the illumination angle for the NW array as compared to film (unpatterned) materials (see Figure 5b). This figure shows that for increasing NW spacings the angular response broadens, retrieving the very broad angular response of individual NWs for sufficiently large spacings. The broad band nature of the absorption spectra as well as the large magnitude of Q_{abs} and the electric field distribution inside each NW in an optimized (130 nm spacing) array also reflect/resemble those of individual NWs (Figure 5c and inset).

From the above discussion, it is clear that the intrinsic and strong optical antenna effects in semiconductor NWs offer a very general and highly effective PM strategy for solar cells. As such, this work complements all the exciting efforts focused on improving the electrical and structural properties of PV materials and NWs. This research could form the basis for a valuable new PV platform technology that is applicable to all semiconductor materials and a wide variety of one-dimensional nanostructures. In addition to the straight, periodic NW arrays discussed here, complex interconnected semiconductor patterns or aperiodic arrays are expected to exhibit similar resonances, opening up a large parameter space for study and optimization. To further boost the performance of these devices, one may also add more conventional PM techniques such as AR coatings and back-reflectors. The required structures are quite large (>100 nm) and can be fabricated using standard, scalable thin film deposition and patterning technologies. Straight NW antennas can also be mass produced and deposited using low-cost procedures such as roll-to-roll ink jet printing on inexpensive plastic substrates. In addition to the exciting possibilities for solar, the technology is quite general and could be applied to ultrafast photodetectors, imagers, sensors, and in reverse for solid-state lighting.

Supporting Information Available. Additional information regarding modeling with Lorentz–Mie formalism and electrostatic dipole absorption. This material is available free of charge via the Internet at http://pubs.acs.org.

REFERENCES AND NOTES

(1) Lewis, N. S. *Science* **2007**, *315*, 798.

(2) Nelson, J., *Physics of Solar Cell*; Imperial College Press: London, 2008.

(3) Kluth, O.; Rech, B.; Houben, L.; Wieder, S.; Schope, G.; Beneking, C.; Wagner, H.; Loffl, A.; Schock, H. W. *Thin Solid Films* **1999**, *351*, 247–253.

(4) Nagel, H.; Aberle, A. G.; Hezel, R. *Prog. Photovoltaics* **1999**, *7*, 245–260.

(5) Zeng, L.; Bermel, P.; Yi, Y.; Alamariu, B. A.; Broderick, K. A.; Liu, J.; Hong, C.; Duan, X.; Joannopoulos, J.; Kimerling, L. C. *Appl. Phys. Lett.* **2008**, *93*, 221105.

(6) Zhao, J.; Wang, A.; Green, M. A.; Ferrazza, F. *Appl. Phys. Lett.* **1998**, *73*, 1991–1993.

(7) Agrawal, M.; Peumans, P. *Opt. Express* **2008**, *16*, 1925–1934.

(8) Catchpole, K. R.; Polman, A. *Opt. Express* **2008**, *16*, 21793–21800.

(9) Bermel, P.; Luo, C.; Zeng, L.; Kimerling, L. C.; Joannopoulos, J. D. *Opt. Express* **2007**, *15*, 16986–17000.

(10) Cao, L.; White, J. S.; Park, J. S.; Schuller, J. A.; Clemens, B. M.; Brongersma, M. L. *Nat. Mater.* **2009**, *8*, 643–647.

(11) Hu, L.; Chen, G. *Nano Lett.* **2007**, *7*, 3249–3252.

(12) Tsakalakos, L.; Balch, J.; Fronheiser, J.; Korevaar, B. A.; Sulima, O.; Rand, J. *Appl. Phys. Lett.* **2007**, *91*, 233117.

(13) Zhu, J.; Yu, Z.; Burkard, G. F.; Hsu, C. M.; Connor, S. T.; Xu, Y.; Wang, Q.; McGehee, M.; Fan, S.; Cui, Y. *Nano Lett.* **2009**, *9*, 279–282.

(14) Fan, Z.; Razavi, H.; Do, J.; Moriwaki, A.; Ergen, O.; Chueh, Y.; Leu, P. W.; Ho, J. C.; Takahashi, T.; Reichertz, L. A.; Neale, S.; Yu, K.; Wu, M.; Ager, J. W.; Javey, A. *Nat. Mater.* **2009**, *8*, 648–653.

(15) Cui, Y.; Lauhon, L. J.; Gudiksen, M. S.; Wang, J.; Lieber, C. M. *Appl. Phys. Lett.* **2001**, *78*, 2214–2216.

(16) Bohren, C. F.; Huffman, D. R. *Absorption and Scattering of Light by Small Particles*; John Wiley & Sons, Inc.: New York, 1998.

(17) ASTM G-173-03. Terrestrial Reference Spectra for Photovoltaic Performance Evaluation; American Society for Testing Materials (ASTM) International: West Conshohocken.

(18) Tian, B.; Zheng, X.; Kempa, T. J.; Fang, Y.; Yu, N.; Yu, G.; Huang, J.; Liber, C. M. *Nature* **2007**, *449*, 885–889.

(19) Palik, E. D. *Handbook of Optical Constants of Solids*; Acadmic Press: London, 1985.

(20) Barber, P. W.; Chang, R. K., *Optical Effects Associated with Small Particles*; World Scientific: Singapore, 1988.

(21) Bandiera, S.; Jacob, D.; Muller, T.; Marquier, F.; Laroche, M.; Greffet, J. J. *Appl. Phys. Lett.* **2008**, *93*, 193103.

(22) Laroche, M.; Albaladejo, S.; Gomez-Medina, R.; Saenz, J. J. *Phys. Rev. B* **2006**, *74*, 245422.

(23) Lalanne, P.; Hugonin, J. P.; Chavel, P. *J. Lightwave Technol.* **2006**, *24*, 2442–2449.